Proceedings of the Combustion Institute 40 (2024) 105466

Contents lists available at ScienceDirect

Proceedings of the Combustion Institute

journal homepage: www.elsevier.com/locate/proci

Experimental and numerical investigation of the induced ignition process in ammonia/air and ammonia/hydrogen/air mixtures

Chunwei Wu [a,*], Yi-Rong Chen [b,c], Van Tinh Mai [b], Robert Schießl [a], Shenqyang (Steven) Shy [b], Chunkan Yu [a], Ulrich Maas [a]

[a] Institute of Technical Thermodynamic, Karlsruhe Institute of Technology, 76131, Karlsruhe, Germany
[b] Department of Mechanical Engineering, National Central University, Taoyuan 32017, Taiwan
[c] Institute of Fluid Science, Tohoku University, 2-1-1 Katahira, Aoba-ku, Sendai, Miyagi 980-8577, Japan

ARTICLE INFO

Keywords:
Ammonia ignition
Hydrogen blending
Minimum ignition energy
Experiments and simulations
Radiation model

ABSTRACT

Ammonia is a prospective fuel for sustainable and clean combustion systems. However, its low reactivity makes ignition and stable combustion difficult, and H_2 addition is considered as a means to enhance the combustion. This study addresses the ignition and initial flame propagation in NH_3 and NH_3/H_2 mixtures by experiment and in simulations. The minimum ignition energy (MIE) is measured in an optically accessible ignition cell. Model simulations of flames evolving from an ignition source involving a detailed treatment of chemical kinetics and molecular transport are performed. Results show that hydrogen addition strongly widens the flammable range of ammonia, and also reduces the MIE. Simulations conducted with and without a radiation model show that radiation strongly influences ignition of ammonia and $10\%H_2/\ 90\%NH_3$ mixture. When radiation is included in the simulations, the predicted flammable range matches experimental observations more closely than without radiation. The results provide an overview of flame initiation and early flame propagation for ammonia/hydrogen mixtures, and highlight the flame enhancement with hydrogen, as well as the importance of radiation in the modeling of ammonia ignition.

1. Introduction

Ammonia is an efficient hydrogen carrier. Ammonia burns without releasing carbon dioxide, and using ammonia as fuel could help to mitigate climate change. Investigating and optimizing ammonia combustion is important for a future net-zero carbon emission society [1], and supports transitioning towards sustainable energy technology.

One of the most significant hurdles met when ammonia is used as a fuel in combustion engines and gas turbines is its low chemical reactivity. This results in a small laminar flame speed ($S_{L,0} \approx 7$ cm/s), and a large laminar flame thickness ($\delta_L \approx 2-3$ mm) near stoichiometry under atmospheric conditions [2–5]. Besides, pure ammonia/air mixtures are difficult to ignite. They feature narrow flammability limits, and are prone to flame extinction. This makes them difficult to use in practical devices [6,7]. Various additives or by-mixtures to ammonia are considered as ignition and combustion enhancers. Hydrogen, with its high reactivity and its potential for causing no CO_2 emission [8], stands as one of the most appealing substances.

Numerous experimental and numerical studies on the combustion of ammonia/air and ammonia/hydrogen/air mixtures have been conducted. Flame speeds [5,9,10], ignition delay times [11,12], and flammability limits [13,14] have been measured. The influence of hydrogen [15–17] addition on ammonia flames has been investigated both experimentally and numerically. Detailed and reduced models of the chemical kinetics of ammonia have been developed (see e.g. [18–20]).

However, there are few studies and data on the transition from induced ignition to a self-sustained flame (or, flame extinction) in ammonia and, specifically, ammonia/hydrogen mixtures. Such data can improve the comprehension of how hydrogen addition to ammonia helps to achieve reliable induced ignition and stable flame propagation, ammonia combustion with improved efficiency and reduced NOx emissions. The Minimum Ignition Energy (MIE) provides crucial information regarding the minimum external energy required for successful flame kernel formation. How to simulate and measure values of MIE for NH_3/H_2/air mixtures and explore possible flammability limits are of fundamental and practical importance.

The questions about the MIE for NH_3/H_2/air mixtures that we want to answer with this study are:

* Corresponding author.
E-mail address: chunwei.wu@kit.edu (C. Wu).

https://doi.org/10.1016/j.proci.2024.105466
Received 4 December 2023; Accepted 17 June 2024
Available online 23 July 2024

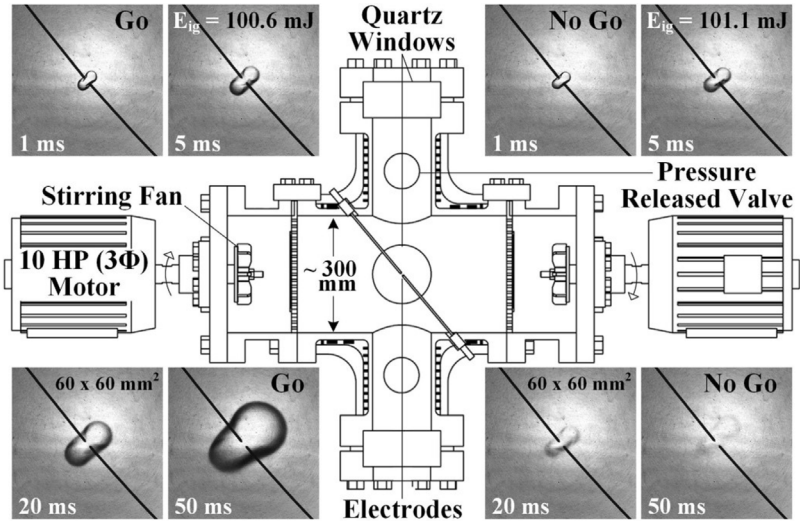

Fig. 1. Schematic of the inner cruciform burner for centrally-ignited, outwardly-propagating laminar premixed flames using a pair of aligned electrodes at the center of experimentation domain. Two sets of the time evolution of NH_3/air schlieren flame images at $\phi = 0.75$ using the same $E_{ig} \approx 101$ mJ are presented, showing that spark ignition is statistical in nature, where "Go" (left images) and "No Go" (right images) events can be co-existed. All images have the same field of view: $60 \times 60\,mm^2$.

- Are the MIE and flammability limits calculated in simulations and measured in experiments comparable?
- What are the factors that impact the accuracy of modeling ammonia ignition?
- How does radiation affect the ignition and early flame propagation process of ammonia and ammonia/hydrogen blends?

In this study, we perform spark ignition experiments and detailed chemistry simulations on the ignition and early flame propagation in mixtures of both pure ammonia and a 90% ammonia + 10% hydrogen blend with air. Our objectives include determining the flammability range and MIE of ammonia, investigating the impact of hydrogen addition on these quantities, and exploring the role of thermal radiation on ignition and flammability in these mixtures, and, as a result, to improve modeling of ammonia ignition and to validate the mechanism of ammonia.

2. Methodology

2.1. Experimental methodology

Values of laminar MIE of NH_3/air and ($90\%NH_3 + 10\%H_2$)/air mixtures over a range of the equivalence ratio (ϕ) at 1 atm and 300 K were measured in a large dual-chamber, constant-pressure, fan-stirred explosion facility. Fig. 1 presents a schematic diagram of the inner cruciform burner having an averaged inside diameter of about 300 mm resided in a large pressure-controlled outer safety vessel (not shown). A pair of counter-rotating fans driven by two identical 10 HP motors together with perforated plates were installed at the two ends of the large horizontal pipe of the cruciform burner, which can be used to generate near-isotropic turbulence in a measurement domain of $150 \times 150 \times 150\,mm^3$ [21,22]. In the laminar induced ignition experiments, fans are used to achieve better mixing and are turned off well before ignition to ensure that the induced ignition occurs in a quiescent mixture. For premixed flame kernel initiation, a pair of stainless-steel 1-mm thickness electrodes with sharp ends were used, which were aligned at 45° angle to the horizon in the center of the measurement domain. Both inner and outer chambers were optically accessible from front to back and from top to bottom. Furthermore, four large pressure released valves were symmetrically installed on the upper and lower vertical tubes of the cruciform burner, so that centrally-ignited, outwardly-propagating premixed flame kernels can be investigated under constant-pressure condition. Detailed information on the setup and the mixture preparation before ignition can be found in our previous studies [21–23].

For the spark ignition system, a precision high-voltage pulse generator (HV-M25K) with a maximum breakdown voltage of 25 kV integrated with adjustable loading resistances and a small damping resistor of 100 Ω in a homemade ignition circuit was used to generate near-square voltage and current waveforms at any controllable pulse duration time varying from 1 μs to a few ms, same as that used in our previous ignition studies [22,23]. The spark with an ignition energy (E_{ig}) of high accuracy measured in situ was discharged from a pair of stainless-steel electrodes of 1 mm in diameter with sharp ends. Here we apply a spark gap of $d_{gap} = 2.0$ mm to reduce heat losses to electrodes. E_{ig} was calculated by the integration of the product of the discharged current $I(t)$ and the voltage difference $[V_1(t) - V_2(t)]$ across the spark gap between electrodes within the pulse duration time of $\tau_p = 500\,\mu s$, where the discharged voltages and current were measured by two high-voltage probes (Tektronix P6015 A) and a current monitor (Pearson Electronics, model 110), respectively. Moreover, high-speed schlieren images of the initial ignition kernel formation and its subsequent development and/or extinction were recorded by a high-speed, high-resolution CMOS camera (Phantom V711) operated at 10,000 frames/s with an exposure time of 1 μs and a resolution of 800 × 800 pixels.

Also, Fig. 1 presents a typical case to display the coexistence of "Go" (left) and "No Go" (right) events by schlieren flame images with a view field of $60 \times 60\,mm^2$ when using the same $E_{ig} \approx 101$ mJ for the NH_3/air mixture at $\phi = 0.75$. For the "Go" case, the flame kernel is developing into a self-sustained laminar expanding flame, while for the "No Go" case, the flame kernel is completely quenched at 50 ms. This confirms that spark ignition is statistical and MIE is a probabilistic variable. In the Supplemental Materials, Fig. S1 and Fig. S2 provide all MIE data points measured at 50% ignitability for this study using the logistic regression method for NH_3/air and ($90\%\,NH_3 + 10\%\,H_2$)/air mixtures, respectively. The interested reader is directed to Ref. [24] for a detailed treatment on the statistical determination of MIE.

2.2. Simulation methodology

The simulations modeling the induced ignition process of pure ammonia and ammonia/hydrogen mixture are performed with an extension of the in-house code INSFLA [25]. With this code, conservation equations for total mass, species mass, energy and momentum

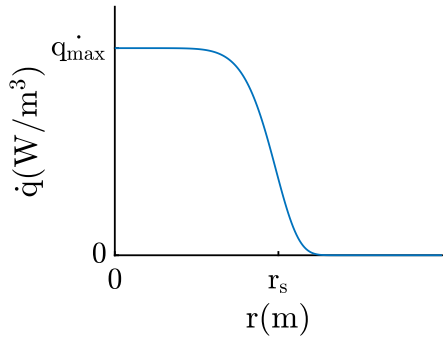

Fig. 2. Spatial dependence of the power density of external source term.

are solved for one-dimensional configurations using detailed chemical kinetics and molecular transport. Both the spatial grid and time-stepping in the code are adaptive; time stepping is coupled to error control. The code delivers profiles of temperature, pressure, and species concentrations, depending on both time and space.

The initial condition of the simulations is set to match the experiments (premixed homogeneous fuel/air mixture, initial temperature $T_0 = 300\,\mathrm{K}$ throughout the whole domain). A constant pressure assumption $p = 1\,\mathrm{bar}$ is applied in all simulations, it was shown that this is a good assumption for ignition duration longer than 20 μs [25], and the ignition duration in the simulation is set to be the same as in experiments, 500 μs. One-dimensional spherical geometry is used in the simulations so that the curvature of the ignition kernel and the evolving flame can be taken into account. Neumann boundary conditions are applied at inner and outer boundaries (zero gradients for species and temperature).

The air and fuel used in the simulations are the same as in the experiments (air: 21% O_2, and 79% N_2; fuel: pure NH_3 or a blend of 90% NH_3 and 10% H_2 by mol). Various fuel/air equivalence ratios within the flammable range are investigated. The chemical kinetics mechanism for ammonia used in the simulations is a detailed chemical mechanism with 34 species and 278 reactions developed by Shrestha et al. [19]. This mechanism reproduces experimental ignition delay times of ammonia well [26], and is very popular for the simulation of ammonia combustion.

Beginning of $t = 0$, an external source term, which is time- and space-dependent, is applied to the conservation equations. The power density $\dot{q}$ of this external energy term has an exponential form, which is a continuous and differentiable function with a nearly rectangular shape, analogous to the experimental source profiles:

$$\begin{aligned} \dot{q} &= \dot{q}_{\max} e^{-\left(\frac{r}{r_s}\right)^8} \quad \text{for} \quad 0 < t \le \tau_s \\ \dot{q} &= 0 \qquad\qquad\qquad\quad \text{for} \quad t > \tau_s \end{aligned} \tag{1}$$

where r_s represents the ignition radius and τ_s is the ignition duration. In this study, $r_s = 1.0\,\mathrm{mm}$, which corresponds to half of the gap of electrodes in experiments, $r_s = \frac{1}{2} d_{gap}$. τ_s is set to be the same value as in the experiments, $\tau_s = 5 \times 10^{-4}$ s. $\dot{q}_{\max}$ is the maximum power density. Fig. 2 shows the spatial profile of the ignition power density.

The total deposited energy E_{ig} during the ignition duration is then:

$$E_{ig} = \int_0^{r_s} \int_0^{\tau_s} 4\pi r^2 \cdot \dot{q} dr dt = \tau_s \cdot \int_0^{r_s} 4\pi r^2 \cdot \dot{q} dr \tag{2}$$

and has a unit of J for spherical geometry.

In both experiments and simulations, flame propagation (caused by chemical reactions) and flame movement (caused by thermal expansion) coexist. To isolate flame propagation, we use the mass-based Lagrangian coordinate Ψ [25], as the mass of the burnt gas increases only when chemical reactions occur. For spherical geometry [27]:

$$\left(\frac{\partial \Psi}{\partial r}\right)_t = \rho r^2 \tag{3}$$

where ρ is the density of the mixture.

Since thermal radiation can play significant role for the flame structure and ignition processes [28], the effect of thermal radiation will also be considered. The simple optically thin approximation model (OTM), which is also used in [28,29], will be considered in the present work. The volumetric radiative heat loss $\dot{q}_{\mathrm{rad}}$ in J/(m^3·s) is given as:

$$\dot{q}_{\mathrm{rad}} = 4 \cdot k \cdot \sigma \cdot \left(T^4 - T_{\mathrm{b}}^4\right), \tag{4}$$

with T_{b} the background temperature. For the present work, $T_{\mathrm{b}} = 300$ K is set to be equal to the temperature of the unburnt gas mixture ($T_{\mathrm{b}} = T_{\mathrm{ub}}$). Moreover, $\sigma = 5.669 \cdot 10^{-8}\,\mathrm{W/(m^2 \cdot K^4)}$ is the Stefan–Boltzmann constant. k is the total Planck mean absorption coefficient, which is determined by considering the contribution of radiation species i as $k = \sum p_i a_{p,i}$, where p_i is the partial pressure of species i in the mixture and $a_{p,i}$ the Planck mean absorption coefficient of radiation species i. According to [28,29], H_2O, NO, N_2O and NH_3 are considered as the four most important radiating species in the ammonia-hydrogen-air system, and their values of the Planck mean absorption coefficient can be found in [29].

The gas mixture in the ignition volume is heated during the ignition duration. After the deposition of ignition energy, a flame kernel may or may not be formed. Moreover, because of the low chemical reactivity of ammonia/air mixture, the heat release of ammonia combustion is relative low, and extinction of the flame kernel may occur because of the strong diffusion for curved flames. In this study, we focus on successful flame propagation, so only a self-sustained flame is considered as a "go" case; ignition failure and flame extinction are both considered as a "no-go" case. This definition of "go" case and "no-go" case is consistent with the experiments.

Fig. 3 shows the temperature profile of a "no-go" case, a "go" case in adiabatic simulations and a "go" case in the simulations with radiative heat loss. The temperature profiles during ignition energy deposition are highlighted in red. Fig. 3(c) uses a different scale compared to Fig. 3(b). In the adiabatic case, flame extinction occurs at 0.005–0.01 s. If the flame survives beyond 0.02 s, it becomes self-sustained; therefore, temperature profiles after 0.02 s are not shown in the figure. In the radiative case, however, the effect of radiation is slow, so it takes much longer to determine if the flame quenches compared to the adiabatic case. Flame extinction might occur at 0.5–1 s, so the temperature profile in Fig. 3(c) is shown up to 1 s. For a "go" case, the propagation of a self-sustained flame is observed, whereas for the "no-go" case, the temperature in the middle drops to 300 K at the end. The MIE in simulations is then defined as the minimum ignition energy required for a "go" case.

Fig. 3(c) shows how the temperature at the center decreases due to radiation while the flame propagates. This is opposite to the adiabatic case in Fig. 3(b), where the temperature at the center stays almost constant after the flame becomes a stable flame (note that the displayed time is different in Fig. 3(b) und in Fig. 3(b)). The reason is that for the radiative case, there is no further heat release by chemical reactions for burnt gas in the center, and the flame front already propagates away from the center. In this case, the heat loss through radiation causes the temperature decrease at the center.

3. Results and discussions

In this section, we will focus on the discussion about the effect of two parameters and models on the MIE from both experimental measurements and simulation results. These two parameters are

(i) Fuel/air equivalence ratio within the lean flammability limit (LFL) and the rich flammability limit (RFL);
(ii) The H_2 content in the NH_3/H_2 mixture is 0% (corresponding to pure NH_3/air mixture) and 10%. We restrict ourselves to those two cases, since each value of MIE is statistically determined in experiments by more than 20 repeated runs using logistic

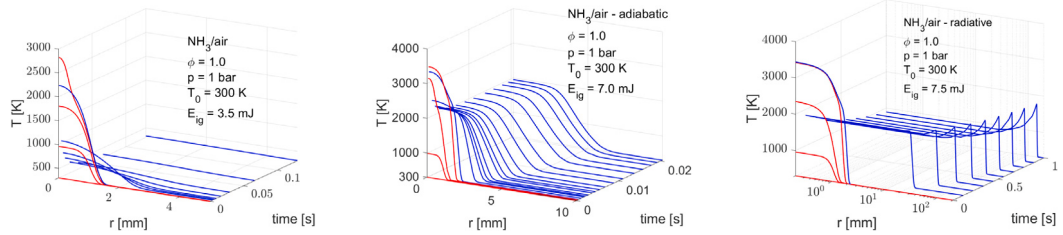

(a) "No-go" case (b) "Go" case - adiabatic (c) "Go" case - with radiation

Fig. 3. The temperature profile of a "no-go" case, a "go" case in the adiabatic simulations and a "go" case in the simulations with radiation heat loss in simulations. Red lines: within spark duration; blue lines: after spark duration. Different times and radii are shown for better visualization in each case. (For interpretation of the references to color in this figure legend, the reader is referred to the web version of this article.)

regression and is very time-consuming. It can be seen that 10% addition of hydrogen already helps the ignition process of ammonia by lowering the MIE and widening the flammable range. In the future, we will also investigate the ignition process of ammonia with higher H_2 blending percentage.

Furthermore, the models considering and neglecting thermal radiation are compared with each other.

3.1. Measured MIE in experiments

Fig. 4 presents measured MIE as a function of ϕ for both pure NH_3/air and (90%NH_3 + 10%H_2)/air mixtures. The uncertainty bars for each MIE datum are also included, which are determined by 95% confident interval using the logistic regression method (please see Figs. S1 and S2 in the Supplementary Materials). Both curves have a "U-shape", which is bounded by LFL and RFL. The LFL and RFL are defined such that a 0.05 decrement (for LFL) or a 0.05 increment (for RFL) of equivalence ratio resulted in 0% successful ignition, even with E_{ig} = 250 mJ, which is 4–8 folds larger than those discharged from typical commercial automobile coils. From this figure, several observations can be made:

- The experimental results of ammonia/air (without H_2 addition) overall have the same tendency as other existing experiments, although their quantitative values can be significantly away even for stoichiometric mixtures. This is because some experimental conditions (e.g. pulse duration time, spark gap width) in former studies are not explicitly mentioned in their work, and the difference of measured values can result from differences in experimental setups.
- Adding hydrogen to ammonia/air mixtures can widen the ignitability range; specifically, from LFL ≈ 0.7 and RFL ≈ 1.25 for pure NH_3 to LFL ≈ 0.45 and RFL ≈ 1.55 for 10%H_2/90%NH_3, respectively.
- Values of MIE for (90%NH_3 + 10%H_2)/air mixtures are noticeably smaller than those of pure NH_3/air mixtures at the same ϕ; MIE drops from 26.9 mJ to 10.5 mJ at $\phi = 1$. The difference becomes exponentially near LFL and RFL of pure ammonia/air mixtures. The decrease of MIE with increasing H_2 addition is also observed in numerical simulation in [30].
- The lowest MIE in the equivalence ratio ranges shift from $\phi = 0.9$ for NH_3/air mixtures to $\phi = 0.75$ when 10% hydrogen is blended, and this tendence is consistent with the numerical results in [30].

3.2. The dependence of MIE on equivalence ratio in simulations and experiments

The dependence of MIE on equivalence ratio in simulations for 0% and 10% H_2, along with the MIE in experiments, are shown in Fig. 5. The LFL and RFL are defined such that a further decrease/increase of

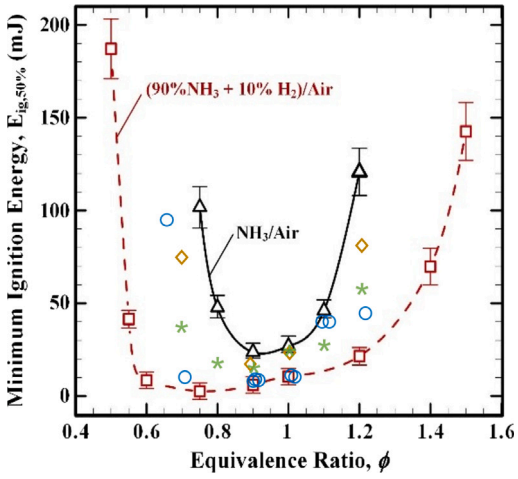

Fig. 4. Laminar minimum ignition energy at 50% ignitability as a function of the equivalence ratio for NH_3/air mixtures (△) and (90%NH_3 + 10%H_2)/air mixtures in volume percentages (□) using a fixed pulse duration time of τ_p = 500 μs. Comparison with other experimental results for pure ammonia are represented by ∘: Verkamp et al. [31]; ∗: Lesmana [32]; ⋄: Sadaghiani et al. [33].

equivalence ratio of 0.01 for LFL/RFL resulted in flame extinction. This occurs even when the ignition energy, E_{ig}, is sufficiently high to heat the mixture up to 10,000 K after ignition.

Furthermore, normalized equivalence ratio is introduced here:

$$\phi_n = \frac{\phi}{\phi + 1} \tag{5}$$

This enables the presentation of both the rich side ($\phi > 1$, $\phi_n > 0.5$) and the lean side ($\phi < 1$, $\phi_n < 0.5$) of the flammable range in a nearly symmetrical manner. [34].

To investigate the impact of thermal radiation on the simulation of ammonia ignition, both MIEs in simulations with and without radiation are shown.

The dependence of MIE on equivalence ratio in simulations, with or without addition of 10%H_2, has a "u-shape" form. This is consistent not only with the experimental results of ammonia, but also with the results of hydrogen and hydrocarbons (see e.g. [25,35,36]).

Besides the "u-shape" form of the dependence of MIE on equivalence ratio, it is also observed that both in experiments and simulations, with the addition of 10% H_2, the flammability range is significantly wider than for pure NH_3/air mixture. At the same ϕ, lower MIE is required for 90% NH_3/10% H_2/air mixtures compared with the MIE for pure NH_3/air mixture. This proves the enhancement of reactivity of ammonia flame with the addition of H_2, which was also observed by Fernandez-Tarrazo et al. [30] through numerical simulation using another reaction mechanism.

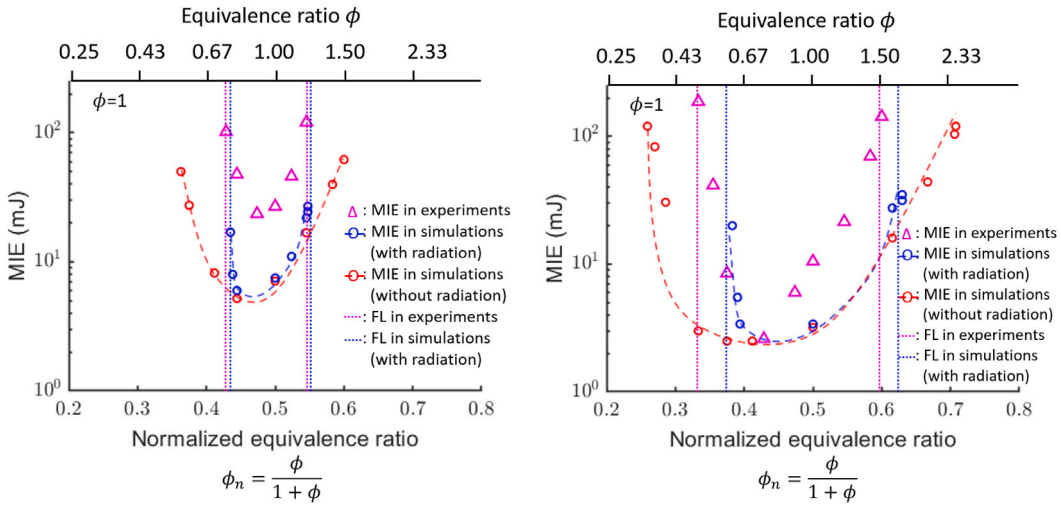

(a) NH_3/air mixtures. (b) 90% NH_3/10% H_2/air mixtures

Fig. 5. The dependence of MIE on equivalence ratio at 1 bar and $T_0 = 300$ K in experiments and simulations for (a) NH_3/air mixtures and (b) 90% NH_3/10% H_2/air mixtures.

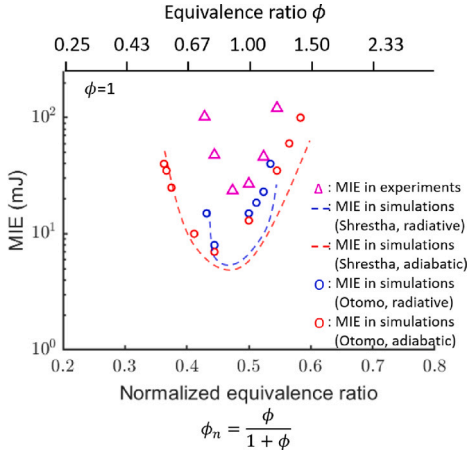

Fig. 6. The dependence of MIE on equivalence ratio at 1 bar and $T_0 = 300$ K in experiments and simulations for NH_3/air mixtures.

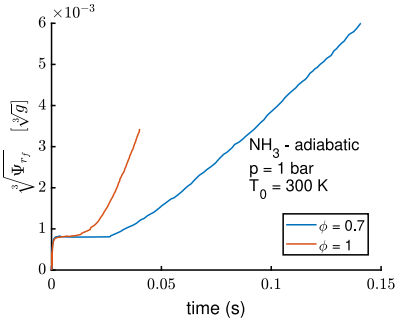

Fig. 7. Temporal evolution of $\Psi_{(r_f)}$ for ammonia flame with $\phi = 1$ and $\phi = 0.7$.

As can be observed in Fig. 5, the flammable range calculated in simulations with radiation is comparable with the flammable range in experiments. Without radiation, however, the flammable range calculated in simulations is larger than in experiments.

In the past few decades, several tens of ammonia mechanisms have been developed. To investigate the influence of the choice of mechanism on the MIE calculated in simulations, we reran the simulations using another mechanism developed by Otomo et al. [37]. The results shown in Fig. 6 confirm that the ammonia flame is very sensitive to heat losses, such as radiation. Although the MIE values calculated with different mechanisms show discrepancies on the rich side, the fact that the flammable range calculated with the radiative model has a better agreement with experiments than the adiabatic model is consistent across both mechanisms. This supports that the underlying physics of the induced ignition of ammonia can be reproduced regardless of the choice of mechanisms.

To investigate the influence of radiation on the ignition process in simulations, MIEs in simulations with or without thermal radiation are performed. The optically thin approximation model (OTM) is considered. Although reabsorption is not included in OTM, and this might influence the MIE value, the predicted tendency of MIE in numerical investigations with OTM can still reveal the importance of radiation for the simulation of forced ignition of ammonia. For the equivalence ratio $\phi = 0.8 - 1$, the MIEs in simulations with or without radiation are comparable. However, with the consideration of thermal radiation, the MIE at ϕ close to LFL/RFL is much larger than that without radiation. To explain this, we investigated the flame propagation caused by chemical reactions. To separate the flame propagation from the expansion of the kernel, we do not use the location of the flame front in the spatial coordinate, but the location in the mass-based Lagrangian coordinate, which is defined in Section 2.2. Ψ_{r_f} represents Ψ at the flame front, which is defined as the distance between the center ($r = 0$) and the peak of the heat release rate. The cubic root of $\Psi_{(r_f)}$ is used here for a spatial indicator. Fig. 7 shows the temporal evolution of $\Psi_{(r_f)}$ for adiabatic ammonia flames with $\phi = 1$ and $\phi = 0.7$, which is close to the LFL. The flame propagation in the adiabatic case is investigated to predict and explain the influence of radiation. In Fig. 7, it can be observed that, after ignition, the flame first propagates at a slow speed. During this critical phase, the heat release through chemical reactions is weak, the flame is very sensitive to heat loss through radiation, flame extinction caused by radiation might occur. After several tens of milliseconds, a self-sustained flame occurs. For the case of $\phi = 0.7$, which is close to the LFL, duration of the critical phase is twice as large as for $\phi = 1$, indicating that the ammonia flame near the flammability limit is more sensitive to thermal radiation than the flame with ϕ near 1.

With 10% addition of hydrogen, as can be seen in Fig. 5(b), the MIEs in simulations and experiments are comparable, at least on the lean side. On the rich side, the calculated MIE in simulations is smaller than in experiments. A possible reason is that the calculated flame speed at the rich side using the chemical mechanism of Shrestha et al. is higher

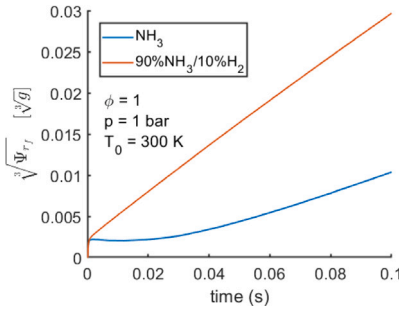

Fig. 8. Temporal evolution of $\Psi_{(r_f)}$ for NH_3 flame and $90\%NH_3/10\%H_2$ flame at $\phi = 1$ with radiation.

than measured in experiments [19]. This discrepancy might result in lower MIEs at the rich side and a larger RFL in simulations.

Even for $\phi = 1$, the MIE of pure ammonia in simulations is 8 times smaller than in experiments. This can be explained as following. As mentioned before, the pure ammonia flame propagates first with a slow flame speed. During this phase, the heat release rate through chemical reactions is slow. Buoyancy (as observed in experiments in Fig. 1) and heat conduction to the cold electrodes become very important and can cause flame extinction. However, as we are using one-dimensional simulations, those effects are not considered. This explains that for pure ammonia, the required MIE for a self-sustained flame in experiments is higher than in simulations. For the case with hydrogen addition, however, as can be seen in Fig. 8, the critical phase where the heat release by chemical reactions is extremely small. The NH_3/H_2 flame propagates at a fast speed from the beginning. In this case, effects like buoyancy and heat conduction to the cold electrodes become less important. The MIEs in simulations and experiments are therefore more similar for $90\%NH_3/10\%H_2$ than that for pure ammonia.

4. Conclusion

As an important characteristic of the ignition process, the minimum ignition energy (MIE) of both NH_3 and $90\%NH_3 + 10\%H_2$ is measured with experiments and simulated with one-dimensional spherical geometry, considering detailed chemical kinetics and detailed molecular transport in this study. The dependence of MIE on equivalence ratio is investigated numerically and experimentally, and the flammable range of NH_3 and $90\%NH_3 + 10\%H_2$ at 1 bar is determined. Moreover, the influence of radiation on the NH_3 and NH_3/H_2 ignition is investigated by modeling.

Results show that both in experiments and simulations, the dependence of MIE on ϕ of NH_3 and $90\%NH_3 + 10\%H_2$ has a "u-shape" form. The MIE is almost independent on ϕ around stoichiometry, and increases rapidly near lean/rich flammability limits. With the addition of hydrogen, the MIE of ammonia decreases, and the flammable range of ammonia widens. This is observed in both experiments and simulations, proving the enhancement of ammonia ignition by addition of small amounts of hydrogen.

An investigation of the influence of radiation on the ignition process shows the importance of incorporating of radiation in the model.

The results in this investigation provide an overview of flame initiation and early flame propagation for ammonia/hydrogen mixtures, and highlight the ignition enhancement by hydrogen, and the importance of radiation in the modeling of ammonia ignition. This has various applications in practical clean combustion engines.

Novelty and significance statement

The novelty of this research is on the minimum ignition energy (MIE) of the NH_3/H_2/air mixture based on both experiment and simulation. It is significant because we include the thermal radiation in the simulation, and confirm that the effect of thermal radiation plays an important role close to flammability limits. We also confirm that the existing mechanisms underpredict the MIE for pure NH_3/air mixtures, while for mixtures with $10\%H_2$ addition the numerical predictions are largely improved.

CRediT authorship contribution statement

Chunwei Wu: Designed research, Performed simulation, Analyzed data, Wrote the paper. **Yi-Rong Chen:** Performed experiments, Analyzed data. **Van Tinh Mai:** Performed experiments, Analyzed data, Plotted figures. **Robert Schießl:** Analyzed data, Methodology discussion, Reviewed the paper. **Shenqyang (Steven) Shy:** Designed experiments, Analyzed data, Reviewed the paper. **Chunkan Yu:** Analyzed data, Wrote the paper. **Ulrich Maas:** Analyzed data, Methodology discussion, Reviewed the paper.

Declaration of competing interest

The authors declare that they have no known competing financial interests or personal relationships that could have appeared to influence the work reported in this paper.

Acknowledgments

The authors gratefully acknowledge the financial contribution from the Deutsche Forschungsgemeinschaft (DFG) under the project MA 1205/32-1, project number 528274426. SSS acknowledges the financial support from the National Science and Technology Council, Taiwan, under grants (MOST 111-2221-E-008-053-MY3 and NSTC 112-2923-E-008-007).

Appendix A. Supplementary data

Supplementary material related to this article can be found online at https://doi.org/10.1016/j.proci.2024.105466.

References

[1] K. Aika, in: K. Aika, H. Kobayashi (Eds.), CO_2 Free Ammonia As an Energy Carrier: Japan's Insights, Springer, Singapore, 2023, pp. 3–16.
[2] H. Kobayashi, A. Hayakawa, K.K.A. Somarathne, E.C. Okafor, Science and technology of ammonia combustion, Proc. Combust. Inst. 37 (1) (2019) 109–133.
[3] P.D. Ronney, Effect of chemistry and transport properties on near-limit flames at microgravity, Combust. Sci. Technol. 59 (1–3) (1988) 123–141.
[4] A.M. Elbaz, B.R. Giri, G. Issayev, K.P. Shrestha, F. Mauss, A. Farooq, W.L. Roberts, Experimental and kinetic modeling study of laminar flame speed of dimethoxymethane and ammonia blends, Energy & Fuels 34 (11) (2020) 14726–14740.
[5] A. Hayakawa, T. Goto, R. Mimoto, Y. Arakawa, T. Kudo, H. Kobayashi, Laminar burning velocity and markstein length of ammonia/air premixed flames at various pressures, Fuel 159 (2015) 98–106.
[6] P. Dimitriou, R. Javaid, A review of ammonia as a compression ignition engine fuel, Int. J. Hydrogen Energy 45 (11) (2020) 7098–7118.
[7] S. Kondo, K. Takizawa, A. Takahashi, K. Tokuhashi, A. Sekiya, A study on flammability limits of fuel mixtures, J. Hazard Mater. 155 (3) (2008) 440–448.
[8] A.A. Konnov, A. Mohammad, V.R. Kishore, N.I. Kim, C. Prathap, S. Kumar, A comprehensive review of measurements and data analysis of laminar burning velocities for various fuel+air mixtures, Prog. Energy Combust. Sci. 68 (2018) 197–267.
[9] U. Pfahl, M. Ross, J. Shepherd, K. Pasamehmetoglu, C. Unal, Flammability limits, ignition energy, and flame speeds in H_2–CH_4–NH_3–N_2O–O_2–N_2 mixtures, Combust. Flame 123 (1) (2000) 140–158.
[10] A. Ichikawa, A. Hayakawa, Y. Kitagawa, K. Kunkuma Amila Somarathne, T. Kudo, H. Kobayashi, Laminar burning velocity and Markstein length of ammonia/hydrogen/air premixed flames at elevated pressures, Int. J. Hydrogen Energy 40 (30) (2015) 9570–9578.
[11] M. Pochet, V. Dias, B. Moreau, F. Foucher, H. Jeanmart, F. Contino, Experimental and numerical study, under LTC conditions, of ammonia ignition delay with and without hydrogen addition, Proc. Combust. Inst. 37 (1) (2019) 621–629.
[12] T. Cai, D. Zhao, S.H. Chan, M. Shahsavari, Tailoring reduced mechanisms for predicting flame propagation and ignition characteristics in ammonia and ammonia/hydrogen mixtures, Energy 260 (2022) 125090.

[13] G. Ciccarelli, D. Jackson, J. Verreault, Flammability limits of NH_3–H_2–N_2–air mixtures at elevated initial temperatures, Combust. Flame 144 (1–2) (2006) 53–63.
[14] M.D. Checkel, D.S.-K. Ting, W.K. Bushe, Flammability limits and burning velocities of ammonia/nitric oxide mixtures, J. Loss Prevent. Process Ind. 8 (4) (1995) 215–220.
[15] D. Wang, C. Ji, S. Wang, J. Yang, Z. Wang, Numerical study of the premixed ammonia-hydrogen combustion under engine-relevant conditions, Int. J. Hydrogen Energy 46 (2) (2021) 2667–2683.
[16] J. Li, H. Huang, N. Kobayashi, C. Wang, H. Yuan, Numerical study on laminar burning velocity and ignition delay time of ammonia flame with hydrogen addition, Energy 126 (2017) 796–809.
[17] J. Chen, X. Jiang, X. Qin, Z. Huang, Effect of hydrogen blending on the high temperature auto-ignition of ammonia at elevated pressure, Fuel 287 (2021) 119563.
[18] A. Konnov, Implementation of the NCN pathway of prompt-NO formation in the detailed reaction mechanism, Combust. Flame 156 (11) (2009) 2093–2105.
[19] K.P. Shrestha, L. Seidel, T. Zeuch, F. Mauss, Detailed kinetic mechanism for the oxidation of ammonia including the formation and reduction of nitrogen oxides, Energy & Fuels 32 (10) (2018) 10202–10217.
[20] R. Li, A.A. Konnov, G. He, F. Qin, D. Zhang, Chemical mechanism development and reduction for combustion of $NH_3/H_2/CH_4$ mixtures, Fuel 257 (2019) 116059.
[21] M.-W. Peng, S.S. Shy, Y.-W. Shiu, C.-C. Liu, High pressure ignition kernel development and minimum ignition energy measurements in different regimes of premixed turbulent combustion, Combust. Flame 160 (9) (2013) 1755–1766.
[22] S. Shy, Y. Shiu, L. Jiang, C. Liu, S. Minaev, Measurement and scaling of minimum ignition energy transition for spark ignition in intense isotropic turbulence from 1 to 5 atm, Proc. Combust. Inst. 36 (2) (2017) 1785–1791.
[23] S. Shy, V. Mai, Y. Chen, H. Hsieh, Nanosecond repetitively pulsed discharges and conventional sparks of ammonia-air mixtures in a fan-stirred cruciform burner: Flammability limits and ignition transition, Appl. Energy Combust. Sci. 15 (2023) 100164.
[24] S.S. Shy, Spark ignition transitions in premixed turbulent combustion, Prog. Energy Combust. Sci. 98 (2023) 101099.
[25] U. Maas, J. Warnatz, Ignition processes in hydrogen-oxygen mixtures, Combust. Flame 74 (1) (1988) 53–69.
[26] L. Kawka, G. Juhász, M. Papp, T. Nagy, I.G. Zsély, T. Turányi, Comparison of detailed reaction mechanisms for homogeneous ammonia combustion, Z. Phys. Chem. 234 (7–9) (2020) 1329–1357.
[27] U. Maas, B. Raffel, J. Wolfrum, J. Warnatz, Observation and simulation of laser induced ignition processes in O_2-O_3 and H_2-O_2 mixtures, Proc. Combust. Inst. 21 (1) (1988) 1869–1876.
[28] M. Faghih, A. Valera-Medina, Z. Chen, A. Paykani, Effect of radiation on laminar flame speed determination in spherically propagating NH_3-air, NH_3/CH_4-air and NH_3/H_2-air flames at normal temperature and pressure, Combust. Flame 257 (2023) 113030.
[29] H. Nakamura, M. Shindo, Effects of radiation heat loss on laminar premixed ammonia/air flames, Proc. Combust. Inst. 37 (2) (2019) 1741–1748.
[30] E. Fernández-Tarrazo, R. Gómez-Miguel, M. Sánchez-Sanz, Minimum ignition energy of hydrogen–ammonia blends in air, Fuel 337 (2023) 127128.
[31] F. Verkamp, M. Hardin, J. Williams, Ammonia combustion properties and performance in gas-turbine burners, Proc. Combust. Inst. 11 (1) (1967) 985–992.
[32] H. Lesmana, Ignition and Combustion Characteristics of Partially Dissociated NH_3 in Air (Ph.D. thesis), The University of Western Australia, 2021.
[33] M.S. Sadaghiani, A. Arami-Niya, D. Zhang, T. Tsuji, Y. Tanaka, Y. Seiki, E.F. May, Minimum ignition energies and laminar burning velocities of ammonia, HFO-1234yf, HFC-32 and their mixtures with carbon dioxide, HFC-125 and HFC-134a, J. Hazard Mater. 407 (2021) 124781.
[34] C.K. Law, Combustion Physics, Cambridge University Press, 2006.
[35] B. Lewis, G. von Elbe, The reaction between hydrocarbons and oxygen, in: B. Lewis, G. von Elbe (Eds.), Combustion, Flames and Explosions of Gases, third ed., Academic Press, San Diego, 1987, pp. 96–211.
[36] C. Wu, R. Schießl, U. Maas, Numerical studies on minimum ignition energies in methane/air and iso-octane/air mixtures, J. Loss Prevent. Process Ind. 72 (2021) 104557.
[37] J. Otomo, M. Koshi, T. Mitsumori, H. Iwasaki, K. Yamada, Chemical kinetic modeling of ammonia oxidation with improved reaction mechanism for ammonia/air and ammonia/hydrogen/air combustion, Int. J. Hydrogen Energy 43 (5) (2018) 3004–3014.